This Paper was awarded the Marshall Fordham Best Research Paper Award at Corrosion & Prevention 2008 for its presentation at Corrosion Control 007.

The Use of Atomic Force Microscopy in Corrosion Research

B. Kinsella[1] & T. Becker[2]

[1]Western Australian Corrosion Research Group,
Department of Applied Chemistry,
Curtin University of Technology, Australia

[2]Nanochemistry Research Institute (NRI),
Curtin University of Technology, Australia

Summary: Atomic force microscopy (AFM), invented in 1986, has found widespread use in science. The technique enables imaging of material at the molecular level for the first time. Unlike most other microscopy techniques, the imaging can be carried out in situ without fear of destroying the integrity of the inter-phase and the process that is being measured. The application of AFM to corrosion science is shown by two examples. The first example concerns the mechanism of adsorption of carbon dioxide corrosion inhibitors (surfactant molecules) on steel. The second example involves an investigation of the mechanism of stress corrosion cracking of weldable 13 chrome steel.

1. Introduction

Atomic Force Microscopy (AFM) was invented in 1986 and commercial instruments became readily available in the early nineties. Development of improved technology and friendlier user approach has seen the technique flourish in many areas of scientific investigation. This paper provides a description of the AFM technique and various modes of operation and its application to corrosion research. Two examples are given – an investigation of the mechanism of adsorption of carbon dioxide corrosion inhibitors and the mechanism of stress corrosion cracking of stainless steel.

2. Scanning Probe Microscopy (SPM)

Scanning Probe Microscopes allow researchers to investigate the topography of a specimen in great detail with a resolution down to the atomic level. The basic principle of these microscopes is a sharp probe that is precisely scanned across the surface of the sample. The probe is moved using a scanner tube made of piezoelectric material that allows accurate positioning. Typically, the scanner tube consists of two parts, one for the lateral and one for the vertical movements. An important advantage of all SPM techniques is the ability to be used in fluid environments, enabling researchers to study samples in-situ, for example biological specimen or the formation of surfactant layers on a sample.

2.1 Scanning Probe Microscopy (SPM)

In 1981 Gerd Binnig and Heinrich Rohrer at IBM, Zurich, invented the first type of a new kind of microscope, the Scanning Tunneling Microscope (STM) (1). Five years later, in 1986, they received the Nobel Prize "for their design of the Scanning Tunneling Microscope". The STM utilises the quantum-mechanical tunneling effect, where a sharp tip (i.e. an etched tungsten wire) is brought in close contact with an electrically conductive or semi-conductive sample. A bias voltage is applied between tip and sample and for a tip-sample (probe-sample) separation of <1 nm a tunneling current of the order of 10^{-9}A can be measured. The tunneling current depends exponentially on the probe-sample separation and can thus be used as a feedback parameter to maintain constant height of the probe above the surface. STMs can be operated in two different imaging modes, the constant height mode and the constant current mode. In constant height mode, the probe is scanned at a constant z-position and the tunneling current varies with topography and with the local surface electronic properties of the sample. In constant-current mode, the microscope uses an electronic feedback to adjust the z-position of the probe relative to the sample in order to maintain a constant tunneling current. In the latter case, the x-, y- and z-data of each point of the scan results in a 3-dimensional topography map of the sample surface.

In 1986, Binnig, Gerber and Quate presented a new form of Scanning Probe Microscope, the Atomic Force Microscope (AFM) (Figure 1). The principle of the AFM is a combination of STM and a stylus profilometer (2). The AFM uses a sharp probe (typical radius of curvature 5-10 nm) mounted on a flexible spring, the so-called cantilever. The deflection of the cantilever is proportional to the force between tip and sample (Hooke's law). Depending on application and imaging mode, cantilevers with a spring constant ranging from 0.01 N/m to 100 N/m are commercially available. The deflection of the cantilever is detected using the beam deflection principle. Here, a laser diode generates a laser beam that is projected on the back of the cantilever and is reflected onto a four-segment photo detector. This technique allows the detection of intermolecular forces such as van der Waals forces. Whereas the STM requires electrically conductive or semi-conductive samples, the AFM is also capable of investigating insulators. AFMs are operated in three different imaging modes: Contact Mode, Intermittent Contact or Tapping Mode and Non-Contact Mode. Contact Mode and Tapping Mode are the relevant imaging modes for the present paper and will be discussed in section 2.2.

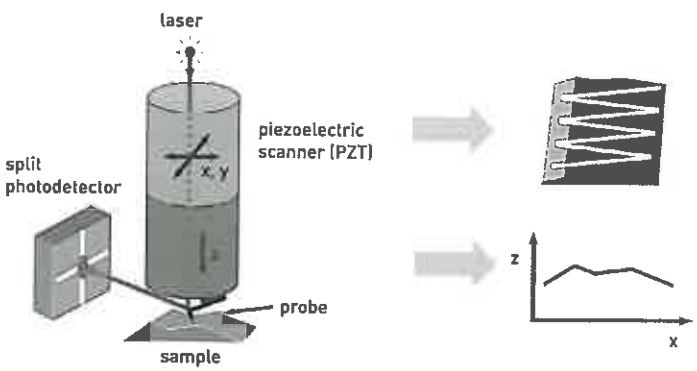

Figure 1: schematic set-up of an Atomic Force Microscope (AFM).

Apart from the operation in any of the above mentioned imaging modes, AFMs can also be used to measure the interaction forces between the probe and the sample. In this mode the tip is moved to a specified lateral position on the sample. The scanner then runs a cycle with the tip approaching from a certain height above the sample into contact and then retracts the tip again. During this cycle the microscope records the force felt by the cantilever and can be used to measure long range attractive or repulsive forces and for investigating local properties like adhesion and elasticity of the sample. In case of Contact Mode operation, the cantilever deflection versus the piezo z-position is recorded and can be transformed and plotted in force distance plots (F-d-plots). Figure 2 shows a typical approach-retract cycle for such a measurement. A similar experiment can be done in Tapping Mode operation. Here, the amplitude of the oscillating cantilever is plotted versus the piezo z-position.

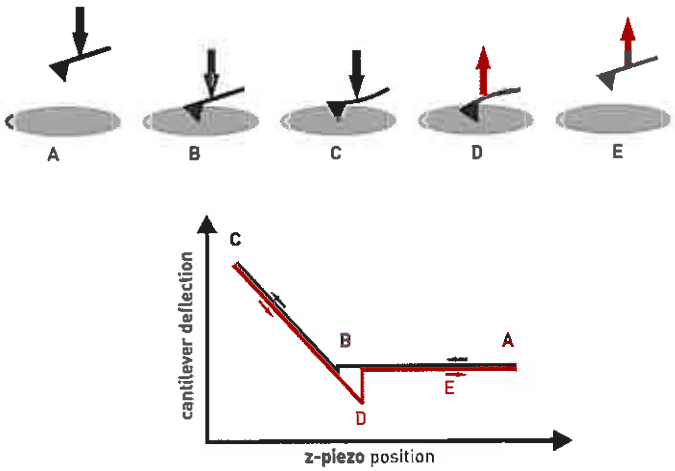

Figure 2: AFM Force Spectroscopy.

Far away from the sample the probe does not feel any forces and the cantilever deflection remains zero (A). As the tip approaches the sample, it eventually touches the sample (B). If the sensitivity is sufficient, short range attractive van der Waals forces can be measured. As the scanner moves further down, the contact force between tip and sample increases linearly (C). During the retraction path the tip sticks to the surface due to adhesion (D). For experiments in ambient conditions, the formation of a capillary neck between probe and sample results in a significantly large adhesive force. To avoid these capillary forces, experiments can be carried out in a nitrogen atmosphere or in solution. Once the pullback force overcomes the adhesive force, the cantilever snaps back into its equilibrium position (E).

2.2 AFM Imaging Modes

The following section describes the imaging modes relevant to the experiments presented in the paper. Contact Mode imaging has been used for the investigation of surfactant layers on mild steel samples. Tapping Mode imaging and Phase Imaging have been applied to the corrosion cracking of stainless steel.

2.2.1 Contact Mode Imaging

In Contact Mode imaging the tip is in permanent contact with the sample surface. The contact force between tip and sample is proportional to the cantilever deflection. Contact Mode cantilevers are usually V-shaped and have spring constants in the range of 0.01-1.0 N/m to avoid damaging the sample. Figure 3 shows a typical silicon nitride Contact Mode cantilever.

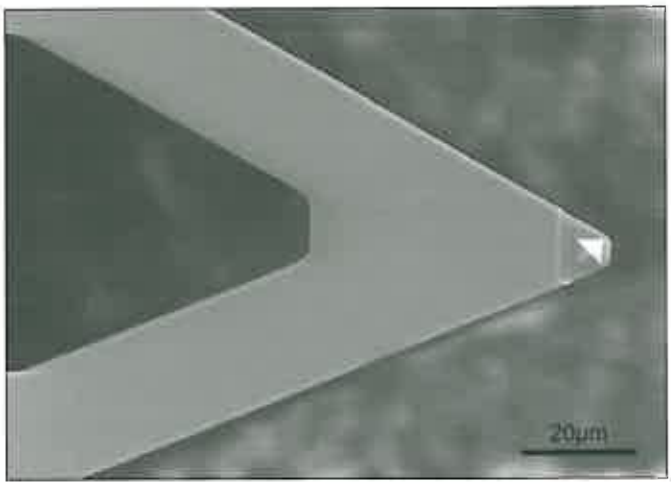

Figure 3: SEM image of a silicon nitride Contact Mode cantilever.

At the beginning of a scan, the scanner moves the tip to the sample until the cantilever is bent a certain amount, which is determined by the user-defined value of the cantilever deflection set-point. This value also defines the contact force for the scan. As the scanner moves the probe across the surface, the tip follows the topography of the sample, which results in a movement of the cantilever. In order to keep the contact force constant throughout the scan, the signal of the photodiode is used as a control parameter for an electronic feedback. The feedback system keeps the laser-spot at a constant position on the photodetector, i.e. the cantilever at a constant deflection resulting in a constant contact force, by moving the scanner in the z-direction. The image of the sample is then generated from the coordinates x, y and z at each point of the scan. A typical scan consists of 512 x 512 pixels. Contact Mode operation is suitable to image hard surfaces like metals and crystals in air and in solutions. The surfaces can be scanned with very high scan rates. On the other hand, Contact Mode imaging is not suitable for the investigation of soft samples like soft polymers or most biological samples because of the relatively large lateral forces the tip exerts on the sample during scanning.

For the investigation of the surfactant films on mild steel presented in this work, the AFM was operated in a so-called "soft contact" mode, which is basically Contact Mode imaging with a very small contact force between tip and sample. This is necessary to make sure that the tip is scanning the surface of the surfactant layer. If the contact force chosen is too large, the tip penetrates the surfactant layer and scans directly the surface of the steel sample. To

provide the correct contact force, a force-distance curve is recorded prior to imaging the sample (see Figure 4). As the tip approaches the sample, the cantilever experiences an increasing repulsive force. The cantilever deflection and thus the force on the surfactant film increases to a maximum value before the tip breaks through the surfactant film. With the scanner moving the tip further down, the tip sample suddenly decreases to zero. This change in separation corresponds to the thickness of the surfactant layer.

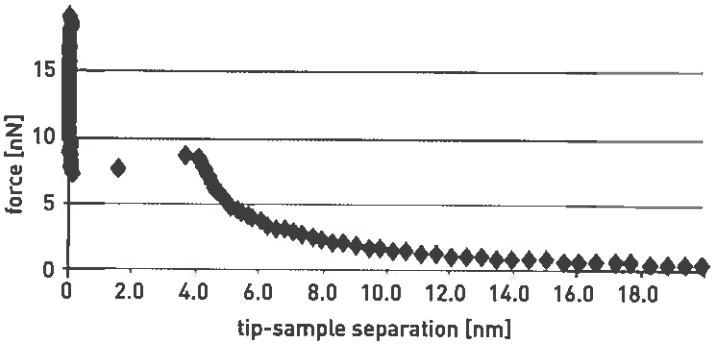

Figure 4: Experimental force-distance plot.

The data were recorded during the approach of the tip to the surfactant layer on a steel sample. As the tip approaches the sample, the contact force increases to about 9 nN, before the tip suddenly breaks through the surfactant layer, which in this case has a thickness of 3.9 nm.

Using the force distance curve it is now possible to determine the maximum contact force that can be applied to make sure that the tip is scanning the topography of the surfactant layer and does not break through the film.

2.2.2 Tapping Mode Imaging

In Tapping Mode, the cantilever oscillates with a frequency close to its resonant frequency near the surface of the sample. The oscillations are generated with a small piezoelectric crystal on which the cantilever chip is mounted in its holder. The amplitude of the cantilever oscillation, which is typically in the order of 20-100 nm, is monitored with the photodiode. In Tapping Mode, also called Intermittent Contact Mode, the tip lightly "taps" on the sample surface at the lowest point of the oscillation cycle. This tapping reduces the free amplitude of the oscillating cantilever. As for Contact Mode, the cantilever deflection is used as a feedback parameter, the amplitude of the cantilever oscillation provides the signal for the electronic feedback, which moves the scanner in z-direction in order to obtain the topography image. The cantilevers used in Tapping Mode are usually much stiffer than the Contact Mode cantilevers. Tapping Mode cantilevers for operation in air are usually made of silicon and have spring constants of 20-100 N/m and a resonant frequency in the range of 50-500 kHz (Figure 5). The large spring constant is necessary to prevent the tip from sticking to the surface during the oscillation. For operation in fluids, the spring constants of Tapping Mode cantilevers are in the range of 0.01-1 N/m.

Figure 5: SEM image of a Tapping Mode cantilever [taken from (3)].

In contrast to Contact Mode, lateral forces are nearly non-existent in Tapping Mode. Thus Tapping Mode is suitable for the investigation of surfaces that are easily damaged or loosely held on the substrate (4), like soft polymers or even surfaces of droplets (5). Imaging is possible in air and in solutions. A disadvantage of Tapping Mode in comparison to Contact Mode is significantly slower scan-speeds.

Phase Imaging

Apart from imaging the topography of a sample, further information about the sample surface can be obtained with so-called Phase Imaging. Phase Imaging is an extension of Tapping Mode AFM, which allows mapping variations for example in adhesion, visco-elasticity or friction. This technique refers to the detection of the phase lag between the driving oscillation generated by the piezoelectric crystal and the response of the cantilever (Figure 6).

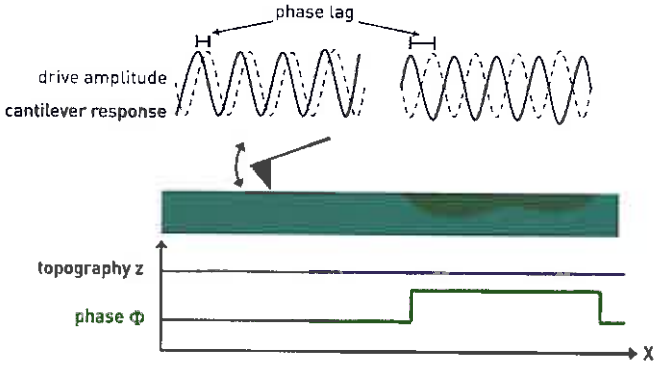

Figure 6: Phase Imaging.

As the probe scans across the flat surface, the z-signal remains constant. In case of a change of the properties of the sample (e.g. from hydrophilic to hydrophobic, represented here in different colours), the microscope picks up a change in the phase lag (adapted from (6)).

Phase Images can also be used for real-time contrast enhancement of the topography images. In the case of

a rough sample large changes in the topography can obscure fine details in the structure of the sample. The phase images are not affected by these height changes and highlight the edges in the topography. This allows imaging the grain structure of even rough samples in great detail and proved to be a powerful tool for the investigation of corrosion cracking in stainless steel.

For the experiments presented in this work, two different AFM systems have been used. The mechanism of carbon dioxide corrosion inhibitors has been investigated with a PicoPlus AFM system (Molecular Imaging/Agilent, USA) operated in Contact Mode. The measurements regarding the stress corrosion cracking of stainless steel have been carried out on a Dimension 3000 AFM equipped with an Extender Module (Digital Instruments, Santa Barbara) operated in both Contact Mode and Tapping Mode. For Contact Mode operation standard silicon nitride cantilevers with a spring constant of k = 0.58 N/m have been used (type DNP, Veeco, Santa Barbara). The Tapping Mode measurements were performed with silicon Tapping Mode cantilevers (type NSC-15, Mikromasch, Spain), which have a spring constant of k = 42 N/m and a resonant frequency of f ≈ 330 kHz. All cantilevers have been treated in an UV-Tip-Cleaner (ATA Scientific Pty Ltd, Australia) for about 30 minutes prior to the experiments.

3. Application of AFM in Corrosion Research

3.1 Mechanism of Carbon Dioxide (CO_2) Corrosion Inhibitors

CO_2 corrosion of mild steel has caused pipeline failure since oil and gas were mined. However, despite the occasional failure the use of mild steel with inhibition still remains a cost effective method of controlling CO_2 corrosion compared to the use of corrosion resistant alloys. In recent years, the depletion of easily accessible supplies, has forced production from much deeper wells. This has resulted in higher fluid temperatures, CO_2 partial pressures and corrosion rates and therefore greater challenges to corrosion inhibitors. The rate of CO_2 corrosion (Equations 1 & 2) can be predicted using the De Waard Millians relationship (Equation 3). The equation shows that the corrosion rate will increase with temperature and increased pressure of CO_2. The CO_2 corrosion mechanism on steel is rapid and occurs much faster than strong acids at the same pH (7).

$$CO_2 + H_2O \rightarrow H_2CO_3 \quad (1)$$

$$H_2CO_3 + Fe \rightarrow FeCO_3 + H_2 \quad (2)$$

$$\log V_c = 7.96 - \frac{2320}{273.2 + t} - \frac{5.55t}{1000} + 0.67 \log P_{CO_2} \quad (3)$$

Where:
V_c is the surface-average rate of metal weight loss (g m^{-2} h^{-1}), which is conventionally converted to mm yr^{-1}

P_{CO_2} is the partial pressure of carbon dioxide, bars

t is the temperature, °C

With well temperatures above 100°C and CO_2 partial pressure >1 bar, corrosion rates >10 mm/yr are commonly predicted. Conventional wisdom is to engineer out the problem down-hole by using corrosion resistant alloys for well tubing, but in large oil and gas flow lines the use of mild steel with inhibition is still more economical. The higher temperatures and pressures have produced new challenges and manufacturers have intensified their research to produce better corrosion inhibitors for these conditions.

CO_2 corrosion inhibitors are surfactant molecules, which feature a polar group joined to a straight chain alkyl group. Molecular models of surfactant molecules are given in Figure 7 (8, 9, -10). The conventional mechanism of these inhibitors is shown in Figure 8. The polar group adsorbs on the steel surface to form a hydrophobic film. The hydrocarbon chain can react with oil and condensate to produce a thicker hydrophobic or oily film. This film prevents the wetting by water and associated carbonic acid.

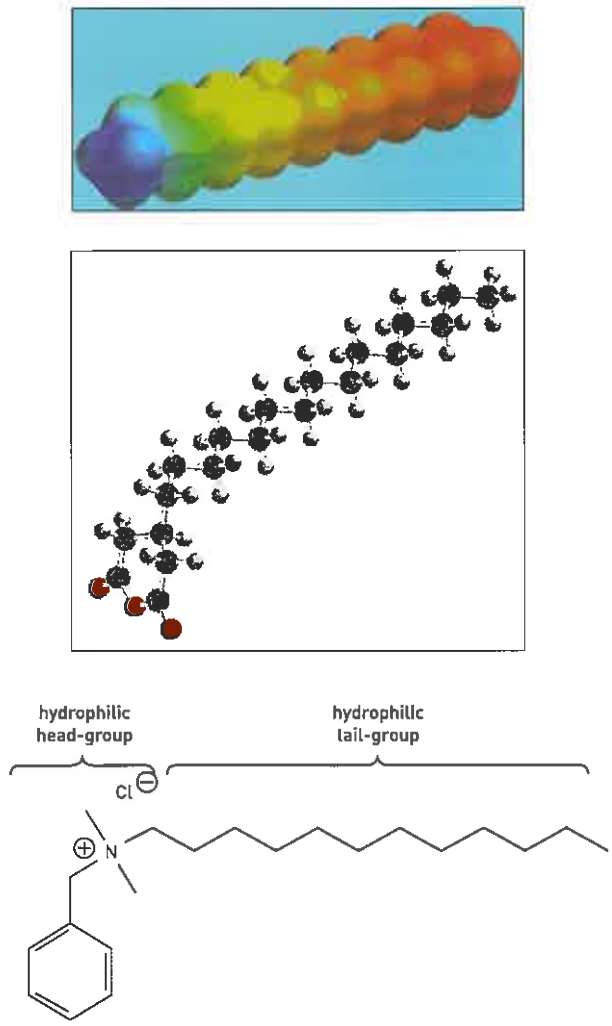

Figure 7: Models of surfactant inhibitor molecules: top *n*-octylamine, middle hexadecyl succinic anhydride which forms a dicarboxylic acid in water, and bottom alkyl benzyl dimethyl ammonium chloride (commercial mixture of C10-C20 alkyl chain length).

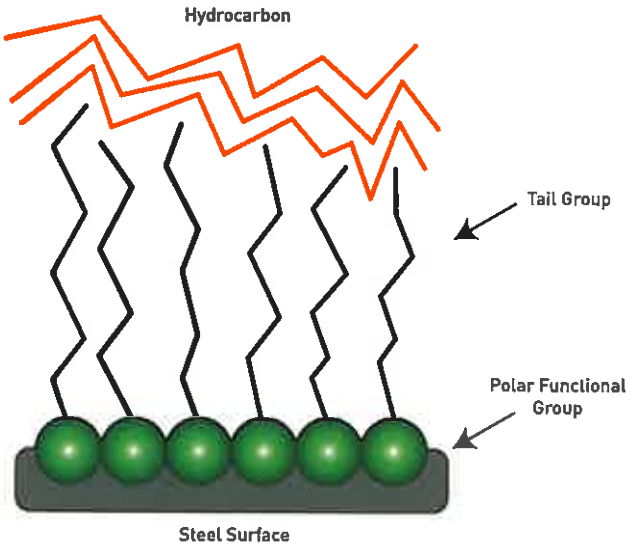

Figure 8: Conventional mechanism of CO_2 corrosion inhibitor adsorption.

The conventional mechanism ignores the fact that surfactant molecules form micelles that can adsorb on the steel surface. It has long been known that highly surface-active materials exhibit unusual physical properties. In dilute solution the surfactant acts as a normal solute, and in the case of ionic surfactants, normal electrolyte behaviour is observed. At fairly well defined concentrations abrupt changes in several physical properties, such as osmotic pressure, turbidity, electrical conductance and surface tension, take place (11). This behaviour can be explained by the formation of micelles of the surfactant ions in which the lipophilic (hydrophobic) hydrocarbon chains are orientated towards the interior of the micelle, leaving the hydrophilic groups in contact with the aqueous solution. The concentration at which micelle formation occurs is termed the critical micelle concentration (CMC). At low concentrations the inhibitor is present as individual ions but at the CMC micelles are formed (Figure 9). Any further addition of surfactant produces more micelles and the concentration of individual molecules remains about the same.

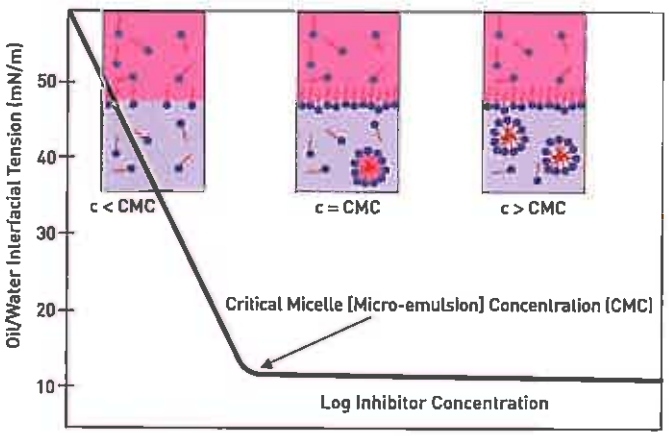

Figure 9: Corrosion inhibitor behaviour in oil water systems.

Recent studies at Curtin indicate that corrosion inhibitors are not effective below the CMC, but their efficiency increases significantly above the CMC. This is shown in Figure 10 where the corrosion rate from weight loss measurements for different inhibitors is plotted as a function of the CMC. The CMC was obtained from measuring the surface tension using the drop weight technique. The surface tension decreases rapidly with increased concentration until the CMC is reached, but at concentrations above the CMC the inhibitor surface tension increases slowly or remains constant. Surfactant scientists have realised that adsorption on solid surfaces is more energetically favourable and takes place after the micelles have formed. The questions are how do micelles adsorb and once they are adsorbed how efficient are they in preventing CO_2 corrosion?

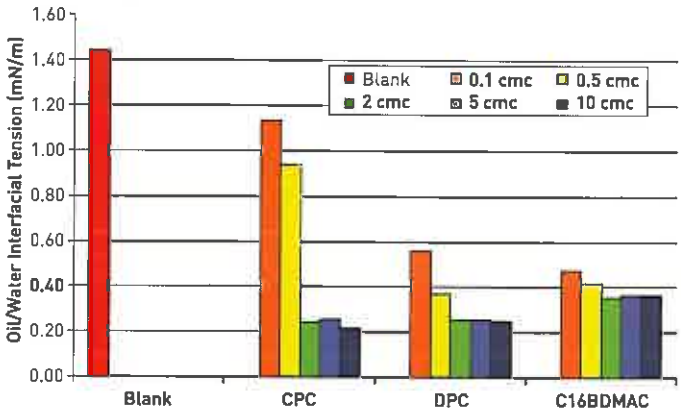

Figure 10: Corrosion rate of carbon steel in CO_2 saturated brine as a function of the corrosion inhibitor CMC; cetyldimethylbenzylammonium chloride (CPC), dodecylpyridinium chloride (DPC) and benzyldimethylhexadecylammonium chloride (C16BDMAC).

Figure 11 shows AFM images of inhibitor molecules on mica obtained using the PicoPlus AFM system in 'soft' contact mode. The advantage of the AFM is clearly shown since the assembly of molecules on a surface can be imaged in the presence of the aqueous phase. Studies to date suggest that the formation of a monolayer or bilayer is better in reducing corrosion. The AFM technique provides a profile of the surface due to molecular adsorption and some indication of depth from the force-distance plots. Little information is obtained on the orientation of the molecules in the adsorbed film. Other techniques such as neutron reflectometry, elipsometry, synchrotron and weight measurements using a quartz crystal microbalance are required to elucidate the orientation of the molecules within the film.

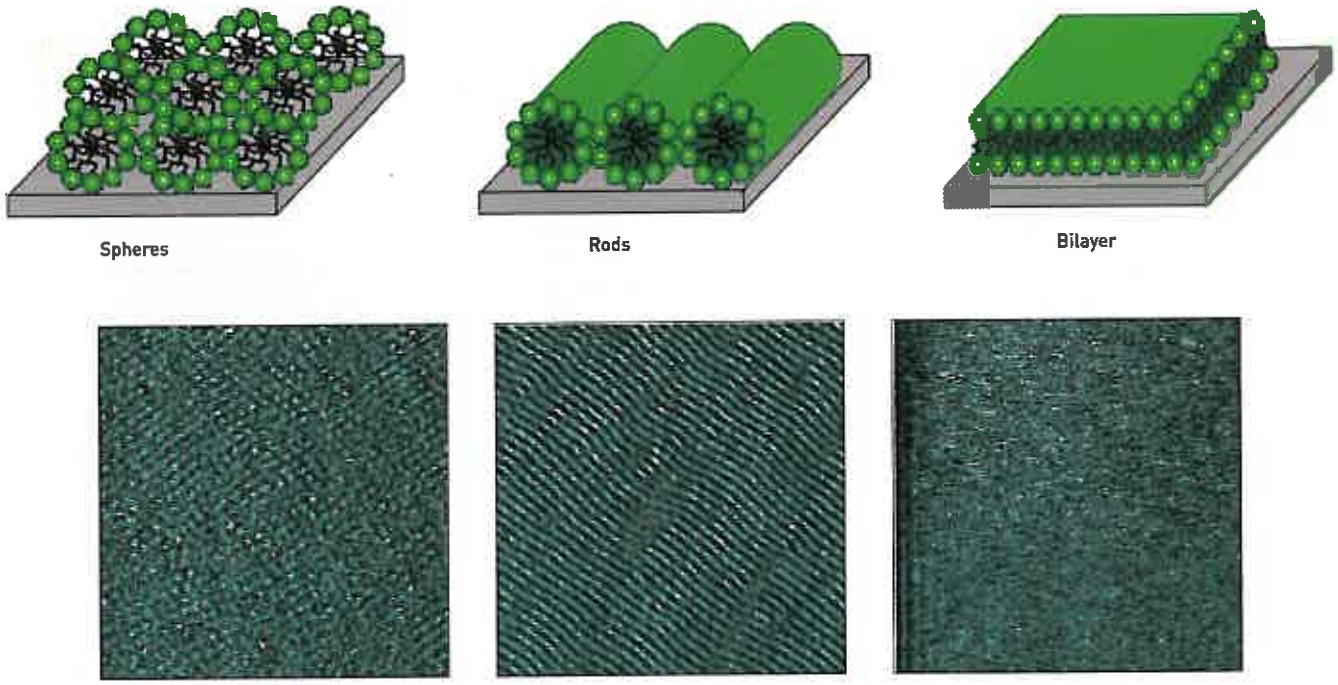

Figure 11: A schematic representation of the three basic shapes (top) that adsorbed aggregates form with their correlating AFM image (bottom); spheres, rods and bilayer (seen as a featureless image). The schematic of the spheres is represented as a cut away image so the orientation of the tail groups can be seen. The surfactant molecules from left to right are dodecylpyridinium chloride, cetylpyridinium chloride and an imidazoline. Images are 300 x 300 nm.

3.2 Stress Corrosion Cracking of Stainless Steel

Oil and gas flow lines made from 13 Cr weldable martensitic stainless steel (WMSS) offer a cost effective alternative to more expensive corrosion resistant alloys, in particular, 22 Cr duplex stainless steel (12, 13, -14). The tubing can be manufactured and laid from large reels and offers a good compromise between cost and resistance to carbon dioxide corrosion. Mainly due to their low nickel content, WMSSs are less expensive than other corrosion resistant alloys and their mechanical properties are superior. However, laboratory tests and field experience indicate the 13 Cr steel undergoes intergranular stress corrosion cracking in the heat affected zone of the welds (12, 13, -14). The use of this steel has been placed on hold pending a greater understanding of the stress corrosion mechanisms.

The 13 Cr steel is produced in three grades:

1. Lean grade, <1% Mo, < 2.5% Ni
2. Medium grade 1-2% Mo, 2.5-4.5% Ni
3. Rich grade, >2% Mo, >4.5% Ni

Lean grades have undergone corrosion cracking in the heat affected zone of the welds. This cracking has taken place both in pipelines and in laboratory tests (13). Chromium carbide has been detected at the grain boundaries and the mechanism is attributed to inter-granular stress corrosion cracking caused by chromium depletion at grain boundaries. For medium and rich grades, the cracking has only been found in laboratory tests. For these grades the mechanism has not been clarified, although it is most likely to be similar to that of the lean grades. Chromium carbide has not been detected at the grain boundaries, but it is speculated that it may exist in narrow bands at the nano-scale level.

AFM has been extensively used in the study of microstructures of materials and environmentally induced fractures (15, 16, -17). The images can be obtained at high resolution at the nano-scale level. However, before using AFM to investigate the mechanism of stress corrosion cracking (SCC) the suitability to detect sensitisation was evaluated using AISI 304L stainless steel. The mechanism of intergranular stress corrosion cracking of 304L stainless steel is well established. Sensitisation is the result of Cr depletion adjacent to the carbides with high Cr content ($M_{23}C_6$, M_7C_3 etc.) formed at grain boundaries (18, 19).

3.2.1 Investigation of Sensitisation of 304L Stainless Steel

The AISI 304L was standard hot rolled 18% chromium, 10% nickel austenitic stainless steel sheet with the elemental composition given in Table 1. Plate specimens

(6 x 6 x 0.3 cm) were cut from sheet and heat treated for different times to create different degrees of sensitisation. The specimens were wet ground with silicon carbide paper in steps of 150#, 240#, 320#, 600#; 800#, 1000#, 1200#, 1500#, 2000#, 2400# and 4000# mesh size by applying faint force to avoid transformation and damage to the samples. They were then polished to a mirror finish using 6 µm, 3 µm and 1 µm diamond suspension. Finally, they were electrochemically polished and etched according to ASTM Standards E1558-9310 and A 262-93a11. The electropolishing solution consisted of 8 vol% perchloric acid, 10 vol% butoxyl ethanol, 70 vol% ethanol, and 12 vol% distilled water at 0°C. The polishing was conducted at 40 V for 20 seconds. The same solution was used by Masao Hayakawa (15, 16) to polish carbon steel to reveal carbides by AFM. The surface etching for AFM observation was controlled to reveal the grain boundaries and be suitable for the height of the AFM tip.

Table 1: Percentage elemental composition of AISI 304L material.

C	Cr	Ni	Mo	Mn	Si	N
0.034	18.33	9.40	0.31	1.22	0.54	0.030

The images presented in the following figures were scanned at a rate of 0.2 Hz. Figure 12 shows AFM micrographs of the six samples of AISI 304L heat-treated at 700°C for different times. The colour contrast in the images indicates the profile across the surface. The bright areas indicate higher regions and the darker areas lower regions or greater etching. The brighter dots or nodules are the carbides formed at the grain boundaries. The carbide particles contain more Cr and are more corrosion resistant. This characteristic causes the particles to project more from the surface after etching. Figure 13 is a three-dimensional (3-D) image of the surface, showing the carbides projecting as spikes from the surface along the grain boundaries.

If the width and length of the carbides is measured, their ratio of occupancy along the grain boundaries can be calculated and used to quantify the degree of sensitisation. Figure 14 shows the ratio of occupancy for the heat treated samples. The carbide size and ratio of occupancy was arbitrarily set to zero for the sample sensitised for 5 minutes, because the carbides were rare to find. The size of the carbides increases with increased heat treatment and sensitisation. In the sample heated for 600 minutes the carbides nodules became almost continuous along some boundaries, indicating severe sensitisation.

After showing that AFM was a suitable technique for detecting sensitisation, the attention then changed to the more difficult task of detecting sensitisation in rich grade, welded, 13Cr martensitic, stainless steel.

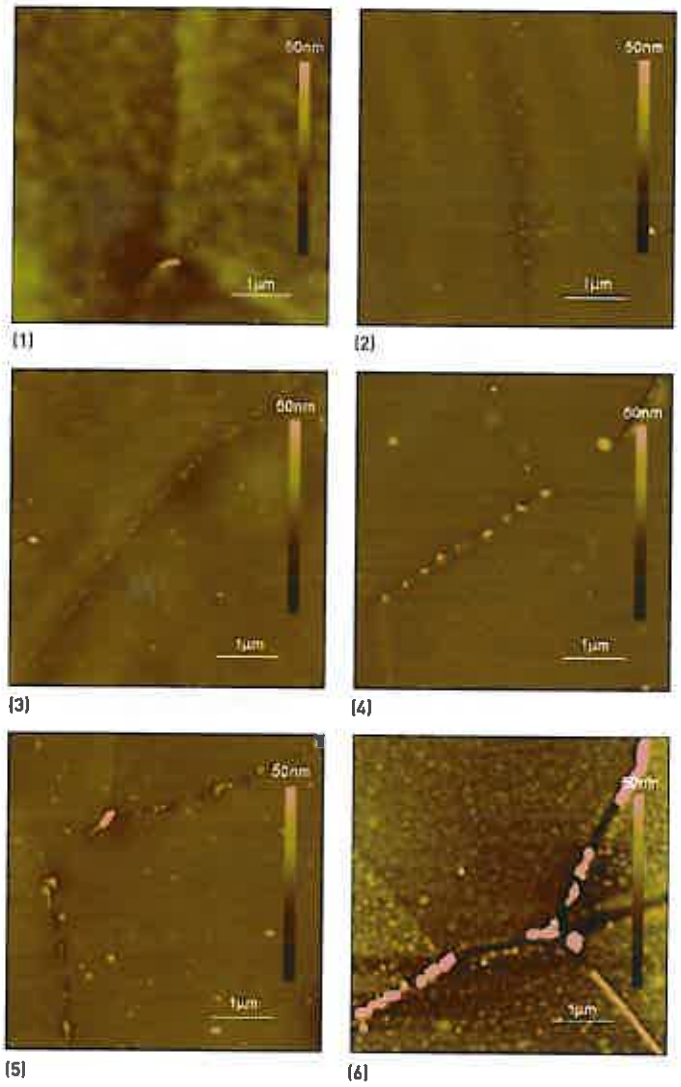

Figure 12: AFM images of the electrochemically etched surfaces. Samples 1-6 were heat treated at 700°C for 5, 15, 30, 60, 300 and 600 minutes respectively.

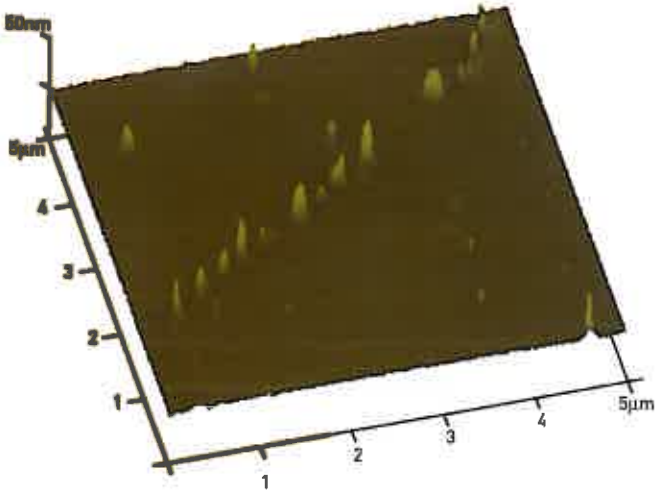

Figure 13: Three-dimensional AFM image of AISI 304L austenitic stainless steel sensitised at 700°C for 60 minutes

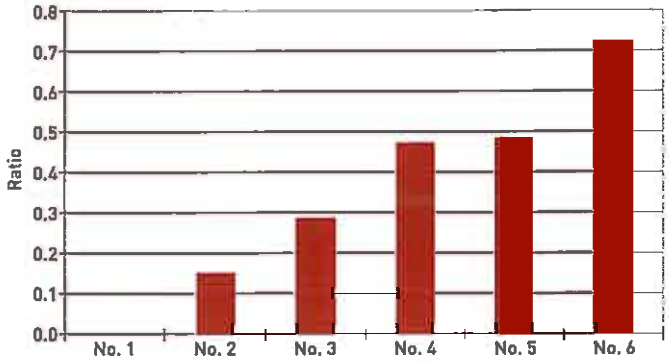

Figure 14: Ratio of carbides occupancy along grain boundaries for 304L samples 1-6, heat-treated at 700°C for 5, 15, 30, 60, 300 and 600 minutes respectively.

3.2.2 *Weldable Martensitic Grade Stainless Steel*

AFM was used to investigate the zone of intergranular attack in the sample of WMSS (Figure 15) that had cracked in a 4 point bend test (Table 2). This zone was located 200 µm from the fusion line and was revealed by visible-light microscopy after electrolytic etching of the polished specimen. Figure 16 shows AFM images of the shallow intergranular attacked zone. An investigation at higher magnification revealed some material projecting out of the surface at former austenite grain boundaries. However, the chemical composition of these surface features remains unclear at present. The assumed corrosion mechanism for medium and rich grade WMSS gives a strong indication that these surface features might be chromium carbide, similar to the tests on the sensitised AISI 304L material. On-going research on this subject is continuing at Curtin and further results are expected to be published soon.

Table 2: Samples of rich grade welded 13Cr martensitic stainless steel investigated for sensitisation to IGSCC. Molybdenum content >2.0 wt% and nickel content >4.5 wt%.

Specimen	Welding condition	Post Weld Heat Treatment (PWHT)	4 Point Bend Test (4PBT) result
A	Off-spec weld (low HI)	No PWHT applied	Cracked
B	Off-spec weld (low HI)	PWHT applied	No cracking found
C	Normal weld	No PWHT applied	No cracking found

Figure 15: Typical sample of welded, rich grade, 13Cr martensitic stainless steel.

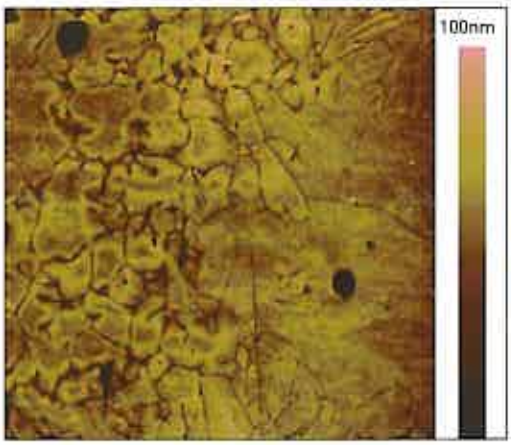

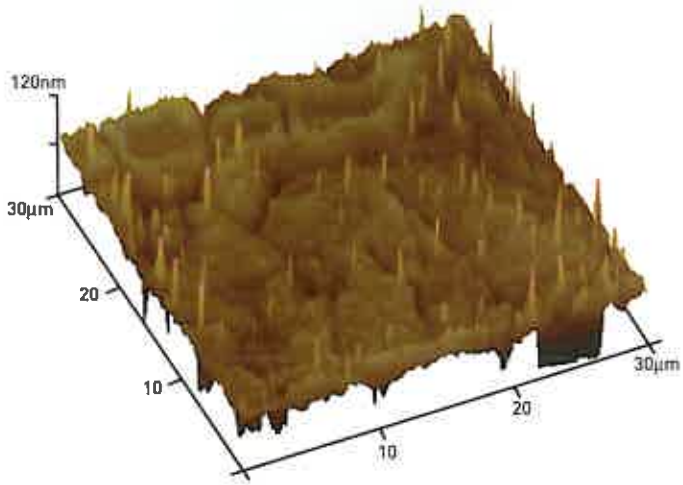

Figure 16: AFM image of cracked sample 200 µm away from fusion line showing intergranular attack as a result of possible sensitisation, tapping mode (100 x 100 µm, 30 x 30 µm).

4. Conclusions

AFM is a very suitable technique for investigations in corrosion science. It is hoped that the two examples given here will inspire researchers to use AFM in other areas of corrosion science, especially to investigate localised forms of corrosion such as pitting and cracking. Although not discussed here, AFM is capable of producing surface potential measurements in air that correlate with the open circuit electrochemical potential in electrolytes. AFM-based surface potential imaging and measurements are able to reveal surface details in unique ways that are useful to corrosion research. These images and measurements, often with nanometre-scale in-plane resolution, are complementary to, and correlate with data from other techniques.

The advantages are:

- images can be obtained at the molecular (nano-scale) level,
- analysis can be performed in situ.

Investigations of metal corrosion carried out in an electrolyte enable potentiostatic control and the initiation of localised forms of corrosion.

5. Acknowledgements

The authors wish to thank Dr Huang Yanliang, for providing the images and information on stress corrosion cracking of stainless steels and PhD student Shandelle Bosenberg for the AFM images of adsorbed surfactant molecules on mica. Dr Huang was a Curtin Visiting Research Scholar, from the Institute of Oceanology, Chinese Academy of Sciences.

6. References

[1] G. Binnig and H. Rohrer, Surface Science, 152/153, p17-26 (1985)

[2] G. Binnig, C.F. Quate, and Ch. Gerber, Physical Review Letters, 56, p930-934 (1986)

[3] Homepage Mikromasch: http://www.spmtips.com

[4] C.B. Prater, P.G. Maivald, K.J. Kjoller, and M.G. Heaton, Veeco Application Note, AN04 (2004)

[5] F. Mugele, T. Becker, R. Nikopoulos, M. Kohonen and S. Herminghaus, J. Adhesion Sci. Technol., 16, pp951-964 (2002)

[6] K.L. Babcock, C.B. Prater, Veeco Application Note, AN11 (2004)

[7] L. S. Moiseeva and O. V. Kuksina, On the Dependence of Steel Corrosion in Oxygen-Free Aqueous Media on pH and the Pressure of CO_2, Protection of Metals, 39, pp490-498 (2003)

[8] W. Durnie, R. De Marco, A. Jefferson and B. Kinsella, Development of a Structure-Activity Relationship for Oil Field Corrosion Inhibitors, Journal of the Electrochemical Society, 146 (5), pp1751-1756 (1999)

[9] W. Durnie, R. De Marco, A. Jefferson and B. Kinsella A Study of the Adsorption Properties of Commercial Carbon Dioxide Corrosion Inhibitor Formulations, J. Appl. Electrochem, 31, pp1221-1226 (2001)

[10] W. Durnie, R. De Marco, B. Kinsella, A. Jefferson and B. Pejcic Predicting the Adsorption Properties of Carbon Dioxide Inhibitors Using a Structure-Activity Relationship, Journal of the Electrochemical Society, 152, B1-B11 (2005)

[11] D. J. Shaw, Introduction to Colloid and Surface Chemistry, Third Edition, Butterworths, UK, Australia, USA (1980)

[12] S. Huizinga and R. K. Ohm, Experiences with Qualification of Weldable Martensitic Stainless Steel Pipe, NACE Corrosion 2003, Paper No.03092

[13] M. E Wilms, et al, Susceptibility of Weldable Martensitic Stainless Steel (13Cr) Pipelines to Internal Cracking, NACE Corrosion 2004, Paper No. 06493

[14] Willem van Gestel, Girth Weld Failures in 13Cr Sweet Wet Gas Flow Lines, NACE Corrosion 2004, Paper No.04141

[15] M. Hayakawa, S. Matsuoka and K. Tsuzaki, Microstructural Analyses of Grain Boundary Carbides of Tempered Martensite in Medium-Carbon Steel by Atomic Force Microscopy, Material Transactions, Vol.43, No.7, pp1758-1766 (2002)

[16] M. Hayakawa, S. Matsuoka, Y. Furuya and Y. Ono, Development of Observation Method for Tempered Martensite Microstructure Using Chemical Mechanical Polishing Technique, Material Transactions, Vol.46, No.11, pp2443-2448 (2005)

[17] K. Minoshima, Y. Oie and K. Komai, In Situ AFM Imaging System for the Environmentally Induced Damage under Dynamic Loads in a Controlled Environment, ISIJ International, Vol.43, No.4, pp579-588 (2003)

[18] M. A. Thomas and G. S. Was, Metal. Trans. A, 21A, pp2097-2107 (1990)

[19] Metals Handbook, Ninth Edition, Vol.13, Corrosion, ASM International, Metals Park, Ohio 44073, Handbook Committee, TA459.M43, 1978, 669 78-14934, ISBN 0-87170-007-7(V.1), SAN 204-7586, p.551